analytical chemistry

Article

Cite This: *Anal. Chem.* 2018, 90, 11531−11537

pubs.acs.org/ac

Scanning Line Probe Microscopy: Beyond the Point Probe

Glen D. O'Neil,[†,§] Han-wen Kuo,[‡] Duncan N. Lomax,[†] John Wright,[*,‡] and Daniel V. Esposito[*,†]

[†]Department of Chemical Engineering, Columbia University in the City of New York, New York, New York 10027, United States

[‡]Department of Electrical Engineering, Data Science Institute, Columbia University in the City of New York, New York, New York 10027, United States

Supporting Information

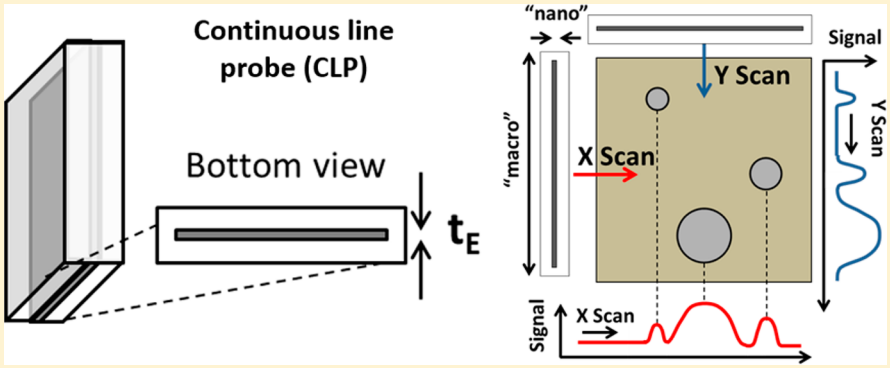

ABSTRACT: Scanning probe microscopy (SPM) techniques have become indispensable tools for studying nano- and microscale materials and processes but suffer from a trade-off between resolution and areal scan rate that limits their utility for a number of applications and sample types. Here, we present a novel approach to SPM imaging based on combining nonlocal scanning line probes with compressed sensing (CS) signal analysis methods. Using scanning electrochemical microscopy (SECM) as an exemplar SPM technique, we demonstrate this approach using continuous microband electrodes, or line probes, which are used to perform chemical imaging of electrocatalytic Pt discs deposited on an inert substrate. These results demonstrate the potential to achieve high areal SPM imaging rates using nonlocal scanning probes and CS image reconstruction.

Downloaded via COLUMBIA UNIV on July 18, 2019 at 18:15:09 (UTC).
See https://pubs.acs.org/sharingguidelines for options on how to legitimately share published articles.

Imaging techniques that allow chemical or physical properties to be viewed at the micro- or nanoscales are of critical importance for fundamental and applied research across the chemical, physical, and biological sciences. Optical microscopy is the oldest and most ubiquitous type of imaging employed in research settings, but its spatial resolution is often limited to the microscale due to the Abbe diffraction limit.[1−3] Scanning probe microscopy (SPM) techniques, such as atomic force microscopy (AFM),[4] enable imaging with significantly higher resolution by using nanoscale "point probes" to locally interrogate the properties of a surface in the immediate vicinity of the probe tip. By scanning the probe over a two-dimensional (2D) area of interest while recording the probe−sample interaction at every (X,Y) location, a high-resolution image of that region may be generated. Despite their powerful capabilities, a major limitation that plagues SPM techniques is a trade-off between areal scan rate (area imaged per unit time) and the spatial resolution of the image. This trade-off results from the sequential, point-by-point sampling method that is required with a conventional scanning point probe. Even with advances in scan patterns,[5−7] post-imaging analysis,[8,9] and advanced tip geometries,[10−13] SPM imaging with point probes is often prohibitively long for imaging areas approaching and exceeding just 1 mm^2.

In the field of signal processing, the one-point-at-a-time measurement scheme employed by today's SPM techniques is considered inefficient, because the information content of a naturally occurring image is almost always far less than the number of "pixels" or points that are sampled in SPM.[14] Herein, we show that the trade-off between imaging resolution, scan area, and scan time may be significantly relaxed if recently developed compressed sensing (CS) signal acquisition methods are used to process SPM measurements obtained using a nonlocal scanning probe that simultaneously records its interaction with a sample surface over many (X,Y) locations. This approach to high-throughput SPM imaging is specifically applied to scanning electrochemical microscopy (SECM), a SPM technique in which electrochemical interactions between a conductive probe and a substrate of interest are monitored as a function of probe location.[15] Conventionally, SECM is performed using a micro- or nanoelectrode as the scanning probe, which consists of an electroactive disc or cone that is sealed in an insulating glass layer (Figure 1A). As in other SPM techniques, this point probe is typically scanned over the area

Received: June 24, 2018
Accepted: August 28, 2018
Published: August 28, 2018

© 2018 American Chemical Society

DOI: 10.1021/acs.analchem.8b02852
Anal. Chem. 2018, 90, 11531−11537

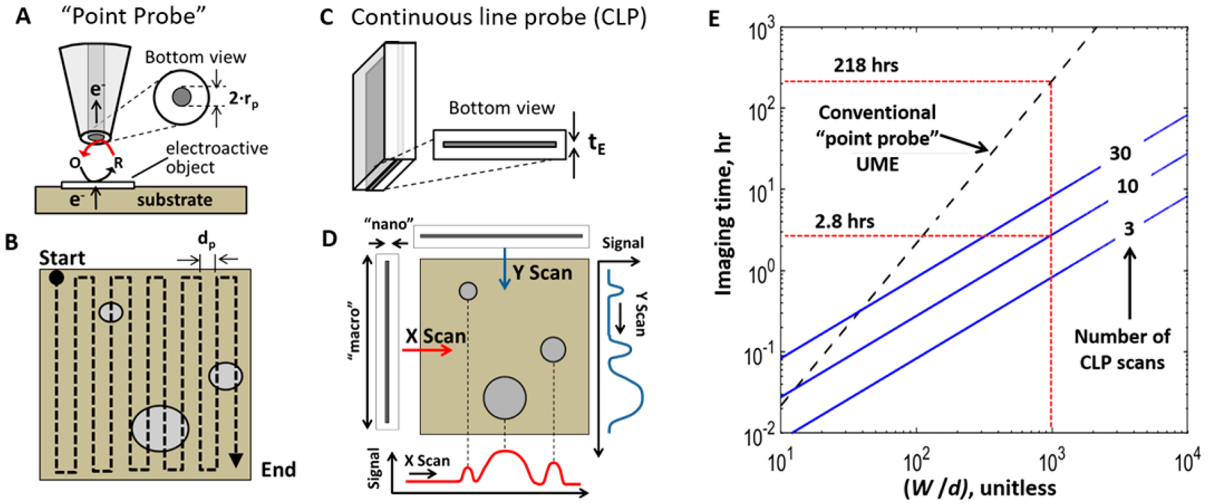

Figure 1. Comparing conventional point probes and continuous line probes (CLPs). (A) Schematic side-view of a conventional point probe UME based on a disc electrode with radius, r_p and (B) a top view of a sample containing three active discs and typical serpentine scan pattern. (C) Schematic side-view of a CLP based on a band electrode with width, t_E, and (D) hypothetical signal output from two scans of a CLP scanned in the *X*- and *Y*-directions. (E) Log–log plot of calculated scan time for SECM imaging of a circular area having diameter (width), *W*, using a conventional point probe (dashed black line) or a CLP (blue solid lines) as a function of the dimensionless ratio of *W* to the desired spatial resolution, *d*. The desired resolution was assumed to be equal to 1.5 times the critical probe dimension ($(2r_p)$ for the point probe or t_E for the CLP) and the probe scan rates were set to $3r_p$ s^{-1} for the point probe and $3(t_E/2)$ s^{-1} for the CLP.

of interest in a serpentine or raster pattern while the interaction between the probe and sample is imaged at every location of interest (Figure 1B). The signal, typically electrochemical current, is plotted as a chemical image that can give useful information about the chemical, physical, electronic, and/or topology of the sample surface.[15−20]

The major advance of this work is to extend SPM imaging beyond "point probes" by employing nonlocal scanning probes, combined with CS, to generate SECM images with significant reduction in scan time compared to conventional SECM. The viability of this approach is demonstrated using a microband electrode, referred to herein as a "continuous line probe" (CLP) (Figure 1C), to image substrates containing sparsely distributed disc electrodes. This study also uses simulated experiments to develop guidelines for the relationship between the minimum required scan time with CLP-SECM and the complexity of the substrate being imaged. Finally, challenges and opportunities for imaging with nonlocal probes and CS image reconstruction are discussed.

EXPERIMENTAL SECTION

Materials. All solutions were prepared using 18.2 MΩ cm water. Concentrated sulfuric acid (Certified ACS plus, Fischer Scientific), sodium sulfate (ACS Reagent grade, Sigma-Aldrich), sodium chloride (ACS Reagent grade, Sigma-Aldrich), and potassium ferrocyanide (Sigma-Aldrich) were used as received without further modification. Platinum foil (99.999%; 250 mm^2) and platinum wire (25 μm diameter) were purchased from Alfa-Aesar. Polycarbonate substrates were obtained from McMaster-Carr. Highly doped, conductive silicon wafers ($p^+Si(100)$) were purchased from WRS wafers (CA).

Preparation of Microelectrodes. Conventional disc-shaped ultramicroelectrodes (UMEs) were prepared by sealing platinum wires in glass capillaries using a laser-based pipet pulling procedure similar to that reported previously.[21] Briefly, platinum microwires (25 μm diameter, Alfa-Aesar) approximately 2 cm in length were attached to Cu leads using silver epoxy (EpoTek H-22) and subsequently placed into borosilicate glass capillaries (Sutter FG-GB100-50-10; o.d. 1 mm, i.d. 0.5 mm). The glass was prethinned using a laser puller (Sutter P-2000) by employing the following program (heat, 350; fil, 3; vel, 35; del, 140; pul, 0). The platinum was sealed in glass after connecting vacuum lines to the open ends of the capillary using Teflon tubing. Two custom 3D printed stoppers were placed between the puller bars and the frame in order to minimize movement of the assembly with respect to the laser. In order to seal the Pt in glass, heat was applied to the capillary for 40 s followed by 20 s of cooling, for three or four cycles (heat, 275; fil, 5; vel, 60; del, 140; pul, 0). After sealing, the stoppers were removed and the hard-pull was accomplished using the following program: (heat, 350; fil, 4; vel, 50; del, 225; pul, 150). After pulling, UMEs were polished at a 30° angle with a home-built polishing system employing 1 μm alumina paper, followed by 0.3 and 0.05 μm alumina slurries, in order to expose the Pt disc. Polishing at a 30° angle ensures that the surface of the disc UME and substrate are parallel for during SECM imaging.

CLPs were fabricated using a procedure similar to that described by Wehmeyer et al. for nanoband electrodes (Figure S1).[22] First, 50 μm thick Pt foil was laminated to an insulating polycarbonate substrate using a two-part 5 min Araldite epoxy (JB Weld). In order to ensure a tight seal with minimal gaps between the Pt and the PC substrate, a vice was used to apply pressure uniformly for several hours while the epoxy cured. The top surface of the Pt foil was electrically insulated using Kapton tape (thickness ≈ 70 μm). The end of the CLP was polished using 1 μm alumina lapping paper (McMaster-Carr), followed by 0.3 and 0.05 μm alumina slurries. Electrodes were characterized with optical microscopy and cyclic voltammetry employing the oxidation of 1 mM $K_4[Fe(CN)_6]$ as a redox probe (Supporting Information). The CLPs exhibit quasi-steady-state behavior at very slow scan rates (2 mV s^{-1}). The slow scan rate is required due to the relatively large size of the band electrodes employed for this study, but the time scale

DOI: 10.1021/acs.analchem.8b02852
Anal. Chem. 2018, 90, 11531−11537

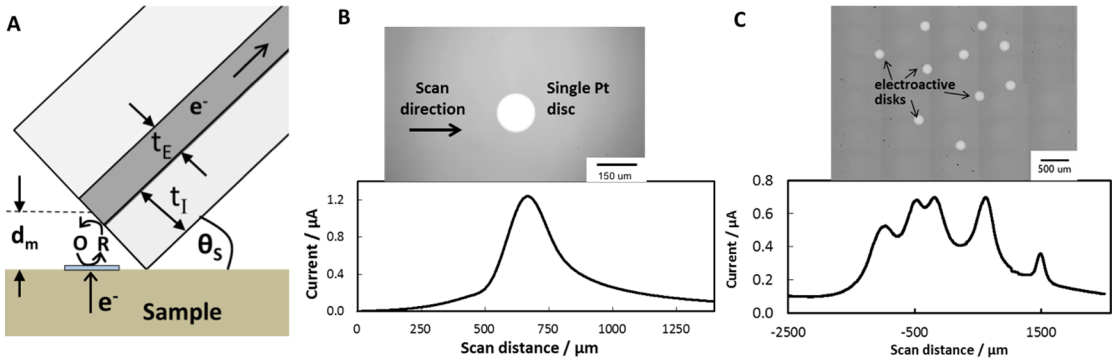

Figure 2. Line scan measurements with a CLP. (A) Cross-sectional side-view of a CLP in contact with a sample surface. The angle of the CLP with respect to the sample surface (θ_{CLP}) and thickness of the bottom insulating layer of the probe (t_I) determine the mean separation distance between the active sensing element and the sample surface (d_m). Amperometric line scan measurements conducted with a Pt CLP (t_E = 50 μm, L_E = 3 mm) scanned at 10 μm s^{-1} over (B) a single electroactive Pt disc and (C) 10 electroactive Pt discs. Both measurements were performed in 1.0 mM H_2SO_4/0.1 M Na_2SO_4 while imaging in substrate-generation, probe-collection mode, whereby H_2 evolved at the Pt discs was oxidized at the CLP.

required to attain a quasi-steady state response is expected to decrease for nanoscale CLPs.

Preparation of Substrates. A set of planar samples containing various patterns of disc electrodes were prepared by evaporating metals (20 nm Pt on 2 nm Ti) onto degeneratively doped p^+Si wafers through a custom-made shadow mask. Pt and Ti were deposited sequentially with an Anstrom EvoVac e-beam deposition system with a base pressure of 1×10^{-7} Torr. Electrical connection to the back of the p^+Si was made by In solder.

Scanning Electrochemical Microscopy (SECM) Imaging. SECM measurements were performed using an SECM system designed around a Renishaw InVia confocal Raman microscope (Figure S2). In this system, an XYZ stage controls the position of the sample relative to the UME or CLP, which is mounted at an angle above the substrate. The UME was mounted in a custom-built probe holder that is attached to an XYZ positioner fixed to dual axis goniometer. Both the XYZ positioner and goniometer are adjusted manually for course adjustment of probe position. The sample stage has maximum travel distances in the XY plane of 4 in. × 3 in. and a minimum step of 0.1 μm in the *X*, *Y*, and *Z* directions. SECM measurements were performed in a low-profile electrochemical cell, which was fabricated from poly(lactic acid) filament using a Makerbot Replicator 2 fused deposition modeling (FDM) 3D printer and screwed into the sample stage. Samples were sealed within the low-profile cell using electroplater's tape (3M). Design files for the probe holder and low-profile cell have been made freely available at echem.io. SECM was carried out with a Ag|AgCl wire as a pseudoreference electrode and a Pt wire coil as the counter electrode. Complete details of the SECM measurement procedures for both conventional and CLP-based SECM can be found in section S1 of the Supporting Information.

RESULTS AND DISCUSSION

Slow imaging speeds are particularly problematic for SECM because the "speed limit" of the scanning ultramicroelectrode (UME) is determined by the time constant associated with diffusion of redox species between the probe and sample. For microscale disc UMEs, this limitation leads to a maximum translational speed of the probe to a few tip radii per second.[6] Combining the scan speed limitation with the facts that (i) the distance between adjacent scans must be equal to or less than the desired resolution, *d*, and (ii) the probe diameter, d_p, must be less than *d*, and it follows that extremely long scan times are required to obtain high-resolution images over large areas. Smaller diffusional time constants can be achieved with nanoelectrodes, but eventually instrumentation constraints such as the response time of the piezo-electric positioners and bandwidth of the electrometer can limit sampling rates.[23]

To illustrate the trade-offs between imaging time, image size, and the desired resolution, SECM imaging times were calculated as a function of the dimensionless ratio of the image width, *W*, to the desired resolution *d* (Figure 1E). The black dashed line shows the result of this analysis for a conventional point probe, and the main assumptions used for the analysis are provided in the figure caption. Taking two values of W/d as examples, Figure 1E predicts that SECM imaging with a point probe at 1 μm resolution over a circular area with diameter of W = 1 mm ($W/d = 10^3$) would require >200 h, while imaging an area with W = 5 mm ($W/d = 5 \times 10^3$) would take >5 400 h. Besides decreasing instrument throughput, long scan times are also undesirable because they increase the likelihood of sample drift and undesirable changes in the sample and/or probe properties, which complicate image interpretation.[24]

In order to demonstrate the viability of nonlocal probes and CS to overcome the trade-off between areal scan rates and resolution, the present study has explored the use of a continuous line probe (CLP) as a nonlocal probe geometry for SECM. One such probe is illustrated schematically in Figure 1C and consists of an active sensing layer that is sandwiched between two insulating layers.[22] This line probe can be fabricated with nano- or microscopic width (for high resolution) and macroscopic length (for large scan area). Importantly, the CLP can simultaneously record electrochemical signal from multiple locations along the length of its active sensing element, resulting in a substantial decrease in imaging time. Figure 1D contains hypothetical signal output for a CLP that is scanned over the same sample area shown in Figure 1B for the point probe but is capable of capturing the same key information (e.g., disc sizes and *X*,*Y* coordinates) in as few as 2−3 scans.

As discussed further below, the exact number of CLP scans required to accurately reconstruct a 2D SECM image from raw line scans strongly depends on sample complexity. Nonetheless, the potential time savings of such an imaging scheme

DOI: 10.1021/acs.analchem.8b02852
Anal. Chem. 2018, 90, 11531−11537

based on a CLP are tremendous, even if 10−50 scans at different angles are required to accurately reconstruct an image. According to Figure 1E, the total imaging times for $(W/d) = 10^3$ and $(W/d) = 5 \times 10^3$ based on 30 CLP scans would be 2.8 and 13.9 h, respectively. Recognizing the potential time savings associated with using a 2D probe, Barker et al.[13] and later Wittstock et al.[10,11] developed an approach using an array of individually addressable microelectrodes that was capable of SECM imaging. Notably, Wittstock et al. were able to image 50 μm features over areas approaching 16 mm^2.[10,11] However, this parallelization approach to SPM imaging comes as the cost of requiring more complex electronics and limited lateral resolution that is limited by the distance between neighboring microelectrodes on the common substrate.[10,11,13]

In the experimental setup employed for this study, the CLP is placed in contact with the substrate at a fixed angle, θ_S, and with a fixed mean distance between the band electrode and the substrate, d_m (Figure 2A). This separation distance is of critical importance for imaging feedback[25,26] and is set by the value of θ_S and the thickness of the insulating layer, t_I, on the bottom-side of the CLP. Such a configuration in which the probe is in physical contact with the substrate may reduce instrument complexity by removing the need for closed-loop positional feedback in the z-direction.[10] In Figure 2B, a simple amperometric line scan carried out by a Pt CLP over a single electroactive disc is shown, providing a distinct peak shape that is consistent with the expected SECM imaging response as the band electrode sweeps over the disc. By analyzing the shape and position of this peak, the location, size, and electrocatalytic activity of the disc may be determined. In other words, the center of the disc electrode may be obtained based on the location of the peak along the scan path, the size of the disc may be determined from the width of the peak, and the electrocatalytic activity of the disc be determined from the magnitude of the peak and probe−substrate separation distance. However, when the CLP is scanned over 10 discs instead of one (Figure 2C), the recorded line scan signal becomes much more complicated because the CLP is simultaneously collecting chemical information that originates from many discs on the sample. Although individual peaks are observed in this line scan, they are highly convoluted, and it is not possible to determine the number of discs or the locations from this single line scan.

Fortunately, recent developments in compressed sensing (CS)[27] provide a powerful means of deconvolving the information contained in CLP scans and reconstructing an SECM image in significantly fewer scans than required with point probe measurements. Compressed sensing methods assume that the image to be reconstructed has a *sparse representation*: it can be expressed as a superposition of a relatively small number of base signals taken from a larger collection, called a dictionary (Figure S5). This principle underlies common signal compression schemes such as JPEG. In the context of CLP-SECM imaging in this work, the dictionary can be thought of as a 2D matrix that describes the response of a point probe UME over a single isolated disc electrode. At a high level, the principle of compressed sensing states that images that have an efficient (sparse) representation can be efficiently and exactly reconstructed from a small number of nonlocal measurements. Moreover, the more efficient the representation, the fewer nonlocal measurements are required to accurately reconstruct the image. Here, the nonlocal measurements are obtained via CLP scans with fixed angles θ_1, ..., θ_S. The image is reconstructed from these measurements by solving an optimization problem, which searches for the simplest (sparsest) image that is consistent with the recorded measurements. Surprisingly, as few as three line scans are sufficient to reconstruct an image when the discs are well-separated and sparse (Supporting Information Sec. S2), which suggests CLP scans can be highly efficient for the signal model employed here.

A demonstration of CS image reconstruction using CLP-SECM measurements is shown in Figure 3 for a sample

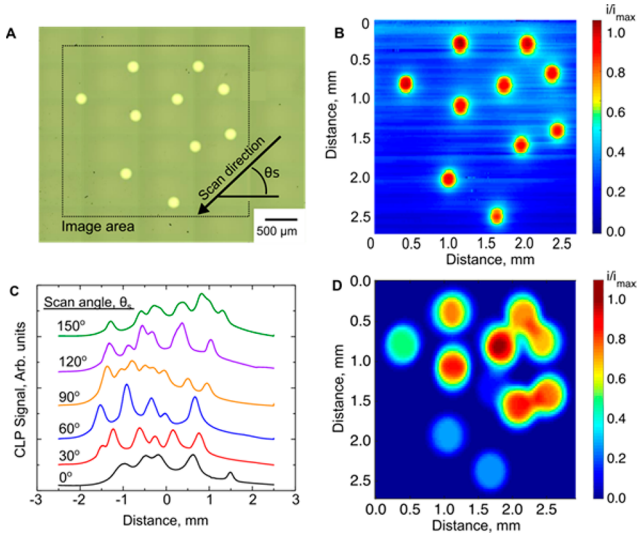

Figure 3. Demonstration of CLP-SECM with CS image reconstruction. (A) Optical image of a sample containing ten 150 μm diameter electroactive Pt discs deposited on an inert p$^+$Si substrate. (B) SECM image of HER activity of sample in part A recorded with a conventional point probe UME (r_p = 9 μm). (C) Individual line scans of sample in part A acquired with a 50 μm × 3 mm CLP. (D) CS reconstructed image of HER activity of sample in part A. All SECM images were recorded in 1 mM H_2SO_4/0.1 M Na_2SO_4 in substrate-generation, probe-collection mode, using a probe scan rate of 10 μm s^{-1} for CLP and point probe SECM measurements.

containing ten 150 μm diameter electroactive Pt discs that were deposited on an inert p$^+$Si substrate (Figure 3A). These measurements were performed with 1 mM H_2SO_4 in substrate generation/probe collection mode, where a negative potential was applied to reduce H^+ to H_2 at the surface of the Pt discs at a diffusion limited rate and a positive potential was applied to the CLP to oxidize H_2 back to H^+. Twelve separate scans were performed by scanning the CLP at different angles across the area of the sample containing the Pt discs. In between each scan of the CLP, the sample substrate was rotated by 15° using a high-precision manual rotation stage. The amperometric response of the CLP is presented in Figure 3C for six of the 12 scans. All 12 of the CLP scans were then processed by CS reconstruction algorithms, as detailed in the Supporting Information section S5, to produce the 2-D chemical image shown in Figure 3D. For comparison, a traditional SECM image was obtained for the same sample using a 20 μm step size and a probe scan speed of 10 μm s^{-1} (Figure 3B), which are the identical conditions for the CLP scans. The slight "streakiness" of the point-probe image can be attributed to the fact that the probe is scanning close to its "speed limit" and may be disturbing the concentration profiles of the electroactive H^+ and H_2 species around the Pt discs. This image

DOI: 10.1021/acs.analchem.8b02852
Anal. Chem. 2018, 90, 11531−11537

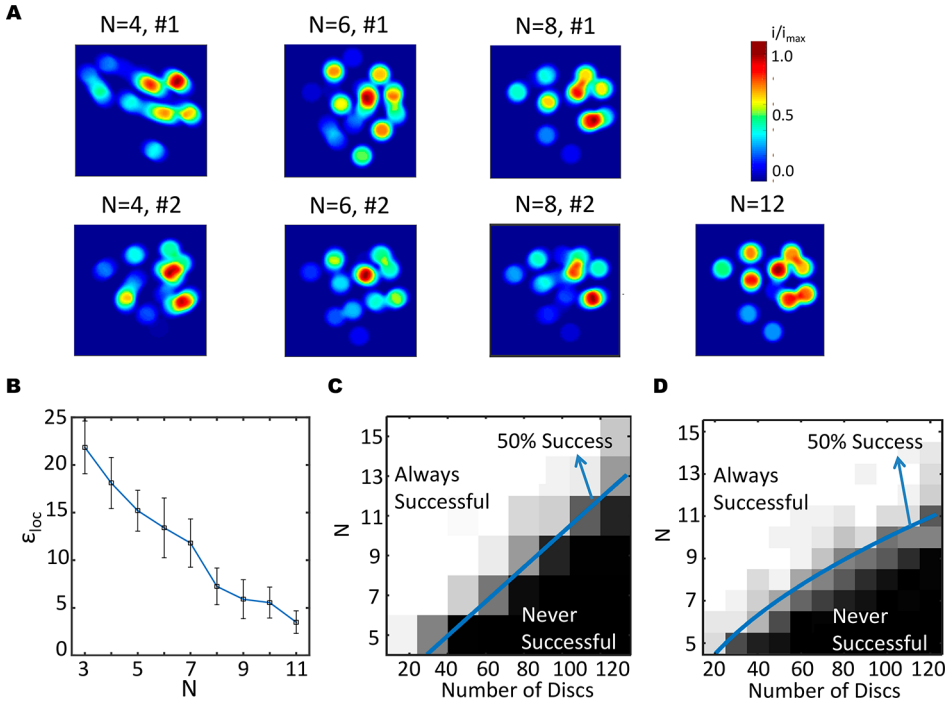

Figure 4. Evaluating the number of scans (N) required for CLP imaging as a function of sample complexity. (A) CS-reconstructed SECM images that were generated using two different combinations of N = 4, 6, or 8 experimentally measured CLP line scans for the sample shown in Figure 3A. (B) Calculated error in disc locations (ε_{loc}) between CS-reconstructed SECM image and the expected SECM image based on the known disc locations, shown as a function of the number of scans used for CS image reconstruction. See text for details on calculating ε_{loc}. CS-reconstruction experiments carried out on hypothetical samples with randomly arranged disc electrode for (C) the case where the number of discs within a set image area is varied and (D) the case where the number of randomly arranged discs is varied while maintaining a constant disc density. For each combination of N and number of discs, the CS image reconstruction algorithm was carried out on 50 different synthetic samples. White pixels represent cases where perfect CS-image reconstruction was achieved in all 50 experiments, while the black pixels represent cases where there was always failure.

required ≈14 h to complete, about an order of magnitude longer than the 80 min it took to perform the CLP-SECM measurements.

It should be noted that the image obtained by the point probe (Figure 3B) has better resolution than that generated with the CLP (Figure 3D); this is largely due to the smaller critical probe dimension of the point probe (d_p = 18 μm) compared to the CLP (t_E = 50 μm). The resolution is expected to become more similar for CLPs with smaller t_E. Additionally, there is significant error in the signal intensities of the CS-reconstructed CLP-generated image, which should give uniform disc intensities as seen for the conventional point probe-generated image (Figure 3B). The signal intensity error in Figure 3D is most likely related to imperfections in the probe geometry, such as warping or protrusions, or probe positioning issues that might lead to a nonuniform probe-substrate separation distance along the length of the CLP. As seen in Figure S4 of the ESI, 10−20% deviations in peak current are recorded when an isolated disc electrode is intersected by a CLP scan at different locations along the length of the CLP. We expect that deviations in relative disc intensities will be substantially reduced when more well-behaved CLPs are used that eliminate or greatly reduce differences in probe sensitivity along its length. Another opportunity to improve the accuracy of the signal intensity is to incorporate knowledge of experimental nonidealities into CS algorithms, which can correct for nonuniform probe sensitivities in a similar way that image post processing of conventional SECM has been applied to correct for blurring caused by fast scan speeds.[9]

Since the major advantage of CLP-SECM over traditional SECM is reduced imaging time, it is important to understand how the number of CLP scans, N, affects the accuracy of the CS-generated image, and whether there is a minimum N required to achieve accurate image reconstruction (N_{min}). The direct relationship between image reconstruction quality and the number of CLP scans is shown in Figure 4A, in which CS reconstructed images were generated using two different combinations of four, six, or eight CLP line scans. While the reconstructions performed with N = 4 scans possess many misplaced and extra discs, it is clear that the number of discs and their locations gradually converge to their true values as N is increased toward 12. This trend is captured quantitatively in Figure 4B, which shows how the error in disc location, ε_{loc}, for a given CS-reconstructed image changes as a function of N. ε_{loc} is defined as the number of false positives (CS-reconstructed discs that do not sufficiently overlap a true disc) plus the number of false negatives (true disc locations that do not sufficiently overlap a CS-reconstructed disc). The procedure for computing ε_{loc} is described in section S6 of the Supporting Information. Figure 4B shows that ε_{loc} gradually approaches zero as N approaches 12, clearly indicating the improved accuracy of reconstruction with increased N.

A more general relationship between the minimum number of scans required for accurate image reconstruction and sample complexity was also studied computationally by performing simulated experiments using synthetic CLP data (Figure

DOI: 10.1021/acs.analchem.8b02852
Anal. Chem. 2018, 90, 11531−11537

4C,D). In both simulations, synthetic samples were generated by randomly arranging varying numbers of electroactive discs of 100 μm in diameter over a defined imaging area such that their center-to-center separation distances were greater than 50 μm. For each synthetic sample, simulated CLP-SECM scans with CLP probe of infinitesimally small thickness were performed employing a randomly chosen scan angle. The number of scans was varied between N = 3 and N = 15 for each experiment, and these synthetic CLP line scans were then fed into the CS reconstruction algorithms to generate images. As shown in Figure S8 in the Supporting Information, the synthetic CLP-SECM images were then compared to the original synthetic samples to see if perfect reconstruction of the SECM image was achieved. Simulations for each combination of N and number of discs were repeated 50 times, and the results are summarized in Figure 4C,D. Two cases were studied in order to elucidate the relationships between sample complexity and required N_{min} in CLP-SECM. In the first case, the effect of "disc density" was evaluated by increasing the number of 100 μm diameter discs within a fixed area of 3 mm × 3 mm (Figure 4C). In the second case, the scan area was varied in each simulation while maintaining a fixed disc density of 20 discs mm^{-2} (Figure 4D). In both Figure 4C,D, the black and white regions of this plot correspond to combinations of N and number of discs for which CS reconstruction was never or always successful in reproducing the true image, respectfully. The gray data points located in between the black and white regions represent combinations of N and number of discs for which the reconstruction was successful for a fraction of the experiments, and the blue solid line is a tie line connecting points for which reconstruction was successful 50% of the time. This tie line can be viewed as a good measure of the minimum number of scans (N_{min}) required to achieve successful image reconstructions.

In Figure 4C, the blue tie line reveals a linear relationship between N_{min} and the number of discs present in the sample of fixed area. As expected, fewer CLP scans are required for successful reconstruction when fewer discs were present in a sample, but as the disc density increases so does N. In comparison with the point probe, which requires constant scanning time for a fixed area, the CLP-SECM enables faster imaging of sparser samples.

For samples with fixed disc density, the tie line in Figure 4D shows that N_{min} increases proportionally to the square root of number of discs, or equivalently, to the square root of image area. This information can be combined with Figure 1E to predict the total imaging time for CLP-SECM. Figure 1E showed that for CLP-SECM, the imaging time is proportional to N_{min} times image length, meaning that the total scanning time will be proportional to the image area for samples with fixed disc density. This linear relationship between total imaging time and image area is the same as traditional point probe. However, the CLP-SECM's coefficient of proportionality is much smaller than that for the conventional disc electrode. Therefore, the CLP-SECM will be more efficient than the traditional point probe regardless of the imaging area, so long as the density of discs on the sample is low enough.

It should be noted that the analysis provided in Figure 4c,d only considers samples containing identical electroactive discs. In theory, CS can also be used to reconstruct images from CLP-SECM line scans of samples possessing electroactive objects with varied sizes, shapes, and intrinsic signal intensities (i.e., heterogeneous local reaction rates). Such samples would require larger dictionaries, but classical theory in CS suggests that this will only lead to a modest increase in the number of line scans needed for accurate reconstruction, since the number of measurements is logarithmic with the size of the dictionary.[28] To demonstrate the ability of CS algorithms to reconstruct images from CLP line scans of more complex samples, a simulated SECM experiment was performed for a sample containing randomly positioned disc electrodes possessing varied intrinsic signal intensities. As seen in Figure S12 in the Supporting Information, CS was able to achieve nearly perfect image reconstruction using only five simulated CLP line scans.

CONCLUSIONS AND FUTURE DIRECTIONS

This study has demonstrated a new approach to SECM imaging that combines the use of nonlocal scanning probes with compressed sensing (CS) signal analysis methods. The major advantage of CLP SECM is its potential to drastically reduce imaging times for SECM imaging over large areas. In general, we expect that CLP-SECM will be useful for applications where the samples of interest are large compared to the desired resolution and are sparsely populated with electroactive objects possessing limited variation in shape and size. For example, high-throughput screening of libraries of electrocatalysts or photocatalysts is one opportunity for immediate application.[29,30] Using CLP-SECM to screen for sparsely populated defects and/or to carrying out low-resolution imaging of large area samples to identify "hot spots" and "cold spots" for high-resolution analysis are other short-term opportunities. However, CLP-SECM will not be applicable for all samples, and considerable advances in both experimental and signal analysis capabilities will be needed if the full potential of CLP-SECM is to be realized.

One future direction will be to demonstrate CLP-SECM with nanoscale resolution. The potential reductions in imaging time are greatest for CLP imaging at the nanoscale, but so too are the challenges that must be overcome to make nanoscale CLP-SECM a reality. For accurate CLP imaging with nanoscale resolution, it will be essential that the band electrode (sensor) of the CLP be positioned parallel to the sample substrate with nanoscale precision. If this condition is not met, significant variation in the probe/substrate separation will exist along the length of the CLP, meaning that the signal intensity for an electroactive object will strongly depend on where it intersects with the CLP. Even a one degree offset between the CLP band electrode and the sample surface can be expected to lead to significant error in the intensities of reconstructed objects. Thus, nanoscale imaging with CLPs will most likely require (i) well-defined CLPs containing band electrodes and insulating layers with thicknesses t_E and t_I, respectively, that are almost perfectly uniform along the entire length of the CLP and (ii) extremely flat sample substrates (see more below), and/or (iii) modified CS reconstruction algorithms that may correct for probe/sample imperfections.

Two other related challenges for CLP-SECM are sample curvature and roughness. Sample curvature can lead to nonuniform probe/substrate separation distances, although flexible CLPs that can remain parallel to the surface during contact-mode scanning offer a promising approach to overcome this challenge. A similar approach has previously been demonstrated for imaging curved and tilted objects using flexible 2D probes based on parallel arrays of point probes.[11,31] Even without curvature, sample roughness and protrusions,

DOI: 10.1021/acs.analchem.8b02852
Anal. Chem. 2018, 90, 11531−11537

especially those that are susceptible to being knocked loose from the surface, can be expected to be problematic for CLP-SECM due to the challenges of using a large probe that is in direct contact with the sample surface.

Despite the limitations of CLP-SECM, we expect that further improvements in CLP imaging methods will greatly improve areal imaging rates for certain sample types and applications. For those applications that CLP-SECM is not appropriate, we hope that this study can inspire researchers to explore other new nonlocal scanning probe geometries, combined with CS, that may overcome inherent limitations of CLP-SECM.

■ ASSOCIATED CONTENT

Supporting Information

The Supporting Information is available free of charge on the ACS Publications website at DOI: 10.1021/acs.analchem.8b02852.

Detailed description of CLP-SECM imaging procedures; description of compressed sensing and image reconstruction algorithm; mathematical model for describing continuous line probe (CLP) scans; mathematical justification of continuous line probes (CLP) as efficient sensors for scanning probe microscopy; algorithm for CS image reconstruction from CLP scans; supporting information for Figure 3 and 4; electrochemical characterization of disc UME and CLP; additional CLP-SECM images; and CS image reconstruction for samples with nonuniform signal intensities (PDF)

■ AUTHOR INFORMATION

Corresponding Authors

*E-mail: de2300@columbia.edu.
*E-mail: jw2966@columbia.edu.

ORCID

Glen D. O'Neil: 0000-0002-2252-779X
Daniel V. Esposito: 0000-0002-0550-801X

Present Address

§G.D.O.: Department of Chemistry and Biochemistry, Montclair State University, Montclair, NJ 07043.

Author Contributions

The manuscript was written through contributions of all authors.

Notes

The authors declare no competing financial interest.

■ ACKNOWLEDGMENTS

The authors would like to acknowledge funding support from the Columbia University SEAS Interdisciplinary Research Seed (SIRS) Funding program and the National Science Foundation Grant Number (NSF Grant CHE-1710400). Any opinions, findings, and conclusions or recommendations expressed in this material are those of the author(s) and do not necessarily reflect the views of the National Science Foundation. The authors would also like to acknowledge Akul Arora for his contributions to the early stages of this project.

■ REFERENCES

(1) Abbe, E. *Arch. für mikroskopische Anat.* **1873**, *9*, 413−418.
(2) Kopelman, R.; Tan, W. *Science (Washington, DC, U. S.)* **1993**, *262*, 1382−1384.
(3) Wu, Q.; Feke, G. D.; Grober, R. D.; Ghislain, L. P. *Appl. Phys. Lett.* **1999**, *75* (1999), 4064−4066.
(4) Binnig, G.; Quate, C. F. *Phys. Rev. Lett.* **1986**, *56* (9), 930−933.
(5) Kiss, A.; Nagy, G. *Electrochim. Acta* **2014**, *119*, 169−174.
(6) Momotenko, D.; Byers, J. C.; McKelvey, K.; Kang, M.; Unwin, P. R. *ACS Nano* **2015**, *9* (9), 8942−8952.
(7) Ziegler, D.; Meyer, T. R.; Amrein, A.; Bertozzi, A.; Ashby, P. D.; Foundry, M.; Berkeley, L. *IEEE/ASME Trans. MECHATRONICS* **2017**, *22*, 381−391.
(8) Kiss, A.; Nagy, G. *Electrochim. Acta* **2015**, *163*, 303−309.
(9) Lee, C.; Wipf, D.; Bard, A. J. *Anal. Chem.* **1991**, *63*, 2442−2447.
(10) Lesch, A.; Vaske, B.; Meiners, F.; Momotenko, D.; Cortés-Salazar, F.; Girault, H. H.; Wittstock, G. *Angew. Chem., Int. Ed.* **2012**, *51* (41), 10413−10416.
(11) Lesch, A.; Momotenko, D.; Cortés-Salazar, F.; Roelfs, F.; Girault, H. H.; Wittstock, G. *Electrochim. Acta* **2013**, *110*, 30−41.
(12) Combellas, C.; Fuchs, A.; Kanoufi, F. *Anal. Chem.* **2004**, *76* (13), 3612−3618.
(13) Barker, A. L.; Unwin, P. R.; Gardner, J. W.; Rieley, H. *Electrochem. Commun.* **2004**, *6* (1), 91−97.
(14) Ganesh, A.; Wright, J.; Li, X.; Candès, E. J.; Ma, Y. *IEEE Int. Symp. Inf. Theory - Proc.* **2010**, *2*, 1513−1517.
(15) Bard, A. J.; Fan, F. R.; Pierce, D. T.; Unwin, P. R.; Wipf, D. O.; Zhou, F. *Science (Washington, DC, U. S.)* **1991**, *254* (5028), 68−74.
(16) Amemiya, S.; Bard, A. J.; Fan, F.-R. F.; Mirkin, M. V.; Unwin, P. R. *Annu. Rev. Anal. Chem.* **2008**, *1*, 95−131.
(17) Mirkin, M. V.; Nogala, W.; Velmurugan, J.; Wang, Y. *Phys. Chem. Chem. Phys.* **2011**, *13* (48), 21196−21212.
(18) Esposito, D. V.; Baxter, J. B.; John, J.; Lewis, N.; Moffat, T. P.; Ogitsu, T.; O'Neil, G. D.; Pham, T. a.; Talin, a. A.; Velazquez, J. M.; et al. *Energy Environ. Sci.* **2015**, *8* (10), 2863−2885.
(19) Polcari, D.; Dauphin-Ducharme, P.; Mauzeroll, J. *Chem. Rev.* **2016**, *116*, 13234−13278.
(20) Mariano, R. G.; Mckelvey, K.; White, H. S.; Kanan, M. W. *Science (Washington, DC, U. S.)* **2017**, *358*, 1187−1192.
(21) Mezour, M. A.; Morin, M.; Mauzeroll, J. *Anal. Chem.* **2011**, *83*, 2378−2382.
(22) Wehmeyer, K. R.; Deakin, M. R.; Wightman, R. M. *Anal. Chem.* **1985**, *57* (9), 1913−1916.
(23) Kang, M.; Momotenko, D.; Page, A.; Perry, D.; Unwin, P. R. *Langmuir* **2016**, *32*, 7993.
(24) Patel, A. N.; Collignon, M. G.; O'Connell, M. a.; Hung, W. O. Y.; McKelvey, K.; Macpherson, J. V.; Unwin, P. R. *J. Am. Chem. Soc.* **2012**, *134* (49), 20117−20130.
(25) Bard, A. J.; Mirkin, M. V.; Unwin, P. R.; Wipf, D. *J. Phys. Chem.* **1992**, *96*, 1861−1868.
(26) Mirkin, M. V.; Wang, Y. Theory. In *Scanning Electrochemical Microscopy*, 2nd ed.; Bard, A. J., Mirkin, M. V., Eds.; CRC Press, 2012; pp 75−125.
(27) Candès, E. J.; Wakin, M. B. *IEEE Signal Process. Mag.* **2008**, *25*, 21−30.
(28) Rauhut, H.; Schnass, K.; Vandergheynst, P. *IEEE Trans. Inf. Theory* **2008**, *54* (5), 2210−2219.
(29) Lee, J.; Ye, H.; Pan, S.; Bard, A. J. *Anal. Chem.* **2008**, *80* (19), 7445−7450.
(30) Haber, J. A.; Cai, Y.; Jung, S.; Xiang, C.; Mitrovic, S.; Jin, J.; Bell, A. T.; Gregoire, J. M. *Energy Environ. Sci.* **2014**, *7* (2), 682−688.
(31) Lin, T.; Lu, Y.; Sun, C.; Pick, H.; Chen, J.; Lesch, A.; Girault, H. H. *Angew. Chem., Int. Ed.* **2017**, *56*, 16498−16502.

DOI: 10.1021/acs.analchem.8b02852
Anal. Chem. 2018, 90, 11531−11537